J Inorg Organomet Polym (2016) 26:62–68
DOI 10.1007/s10904-015-0281-7

Syntheses, Structures and Catalytic Properties of Cobalt(II) and Silver(I) Coordination Polymers Based on Flexible Bis(2-methyl benzimidazole) and Dicarboxylic Acids

Xu Zhang[1] · Gui-Ying Dong[1] · Yong-Guang Liu[1] · Guang Hua Cui[1]

Received: 8 July 2015 / Accepted: 14 September 2015 / Published online: 18 September 2015

Abstract Two coordination polymers formulated as $[Co_2(2,6\text{-ndc})_2(L)]_n$ (**1**) and $[Ag(L)(1,4\text{-Hndc})]_n$ (**2**) (L = 1,1′-(1,4-butanediyl)bis(2-methylbenzimidazole), 2,6-H_2ndc = 2,6-naphthalenedicarboxylic acid, 1,4-H_2ndc = 1,4-naphthalenedicarboxylic acid) were synthesized under hydrothermal conditions and characterized by IR, elemental analysis, and single-crystal X-ray diffraction. The structural analysis reveals that complex **1** exhibits an unprecedented 3D framework with threefold interpenetrating **xah** topology. Complex **2** shows a 1D "Ω"-like chains bridged by L ligands, which is further extended via O–H···O hydrogen bonding interactions into a 2D (4,4) supramolecular layer. The thermal stability and catalytic properties of two complexes for the degradation of Congo red dye in a Fenton-like process was also investigated.

Keywords Bis(benzimidazole) · Crystal structure · Catalytic property · Paddle-wheel

1 Introduction

The design and synthesis of novel metal–organic coordination polymers (MOCPs) have attracted an increased attention for their structural diversity and their promising applications as various functional materials [1–4]. The self-assembly of MOCPs with expected structure and properties is still faced with many difficulties, because the structure of complexes may be easily affected by organic ligands, metal ions, solvent, reaction temperature, counterions. Among them, the selection of appropriate multifunctional ligands as building blocks is crucial to determine the structural outcome of target MOCPs [5–7]. The flexible bis(benzimidazole) derivatives, which can satisfy the coordination needs of the metal centers and consequently generate more robust and intricate networks, have attracted much attention and been widely used as classical N-based ligands [8–11].

The metal coordination polymers based on aromatic dicarboxylate have been extensively investigated in the past decades due to their strong coordination capability, large conjugated-system and the possibility of offering new functional materials [12, 13]. The 2,6-naphthalenedicarboxylic acid(2,6-H_2ndc) and 1,4-naphthalenedicarboxylic acid (1,4-H_2ndc) are typical aromatic dicarboxylic acids, have attracted tremendous attention in constructing MOCPs with elegant architectures and desired properties, which can be attributed to its various coordinating modes, high symmetry and structural rigidity [14–18]. However, the studies on the effect of these aromatic dicarboxylates on the structures and properties of ternary mixed-ligand complexes based on the flexible bis(2-methybenzimidazole) ligands are still limited in literatures. In continuation of this theme, we employed 2,6-H_2ndc, 1,4-H_2ndc, and 1,1′-(1,4-butanediyl)bis(2-methylbenzimidazole) (L) as co-ligands, two uncommon metal coordination polymers have been obtained under hydrothermal conditions, namely, $[Co_2(2,6\text{-ndc})_2(L)]_n$ (**1**) and $[Ag(L)(1,4\text{-Hndc})]_n$ (**2**). Moreover, the thermal stability and catalytic properties of **1** and **2** have also been presented in detail.

✉ Gui-Ying Dong
tsdgying@126.com

✉ Guang Hua Cui
tscghua@126.com

[1] College of Chemical Engineering, North China University of Science and Technology, Tangshan 063009, Hebei, People's Republic of China

2 Experimental Section

2.1 Materials and Physical Measurements

The L ligand was prepared according to literature procedures [19]. The other reagents were purchased from Sinopharm Chemical Reagent Co, Ltd. and used without further purification, C, H, and N elemental analyses were performed with a Perkin-Elmer 240C analyzer. The IR spectra were recorded from 4000 to 400 cm^{-1} using an FTIR Avatar 360 (Nicolet) spectrophotometer as a KBr pellet. The TG measurements were carried out with a Netzsch TG 209 thermal analyzer from room temperature to 800 °C under N_2 with a heating rate of 10 °C min^{-1}. The X-ray powder diffraction (XRPD) patterns were recorded on a Rigaku D/Max-2500 diffractometer at 40 kV, 100 mA for a Cu-target tube and a graphite monochromator. The absorptivity value of Congo red was recorded with a Shanghai Jingke 722 N spectrophotometer at the maximum wavelength of 496 nm.

2.2 Synthesis of $[Co_2(2,6\text{-ndc})_2(L)]_n$ (1)

A mixture of $CoCl_2{\cdot}6H_2O$ (24 mg, 0.1 mmol), L (64 mg, 0.2 mmol), NaOH (8 mg, 0.2 mmol), 2,6-H_2ndc (43 mg, 0.2 mmol) and 10 mL water was heated at 140 °C for 3 days in a Teflon-lined vessel (25 mL). After the mixture cooled to room temperature at a rate of 5 °C h^{-1}. Purple block single crystals suitable for X-ray diffraction was collected by filtration. Yield: 40 % (based on $CoCl_2{\cdot}6H_2O$). Anal. Calcd for $C_{22}H_{17}CoN_2O_4$: C, 61.12; H, 3.96; N, 6.48 %. Found: C, 61.29; H, 3.49; N, 6.29 %. IR (KBr, cm^{-1}): 1620s, 1510s, 1460s, 1290s, 1190m, 916w, 773m, 559w.

2.3 Synthesis of $[Ag(L)(1,4\text{-Hndc})]_n$ (2)

Complex **2** was prepared in the same way as that for **1**, except using $AgNO_3$ (34 mg, 0.1 mmol) and 1,4-H_2ndc (43 mg, 0.2 mmol) instead of $CoCl_2{\cdot}6H_2O$ and 2,6-H_2ndc. Colorless block crystals of **2**, suitable for X-ray diffraction, were acquired at a yield of 62 % based on $AgNO_3$. Anal. Calcd for $C_{32}H_{29}AgN_4O_4$ (641.46): C 59.92, H 4.56, N 8.73 %; found: C, 59.60; H, 4.79; N, 8.43 %. IR (KBr, cm^{-1}): 1690m, 1650s, 1520s, 1420s, 1350m, 741s.

2.4 Single Crystal X-ray Diffraction Determination

Crystallographic data for complexes **1–2** were collected on a Bruker Smart CCD diffractometer with Mo–Kα radiation ($\lambda = 0.71073$ Å) using ω-2θ scan mode at 293(2) K. Absorption corrections were applied by using the multiscan program SADABS [20]. The structures were determined by direct methods and refined on F^2 full-matrix least-squares using the SHELXTL-97 program package [21]. All of the non-hydrogen atoms were refined anisotropically. The hydrogen atoms were assigned with common isotropic displacement factors and included in the final refinement by using geometrical restrains. The crystallographic data for the crystal structure is summarized in Table 1, and the selected bond lengths and angles are listed in Table 2.

3 Results and Discussion

3.1 Crystal Structure of $[Co_2(2,6\text{-ndc})_2(L)]_n$ (1)

The X-ray crystallographic analysis shows that the complex crystallizes in the triclinic space group $P\bar{1}$, there are one crystallographically independent Co(II) atom, one-half L ligand and two distinct halves of 2,6-ndc^{2-} ligand in the asymmetric unit. As shown in Fig. 1a, the Co(II) atom is five-coordinated by one nitrogen atom(N1) from one L ligand and four oxygen atoms [$O1^i$, O2, O3A, O4, Symmetry code: (i) $-x, -y + 1, -z + 1$] from four distinct 2,6-ndc^{2-} ligands giving rise to a square-pyramidal coordination geometry with the τ parameter being 0.046 [22]. The Co–N bond length is 2.092(2) Å and the Co–O ones vary from 2.029(2) to 2.092(2) Å.

In the structure **1**, the 2,6-ndc^{2-} ligands adopt the μ_4-$\eta^1{:}\eta^1{:}\eta^1{:}\eta^1$ coordination mode, four carboxylate groups of four 2,6-ndc^{2-} ligands bridge two Co atoms into a binuclear $[Co_2(COO)_4]$ paddle-wheel unit with non-bonding Co(II)···Co(II) separation of 2.9943(6) Å. Neighboring $[Co_2(COO)_4]$ units are further bridged by 2,6-ndc^{2-} ligands to give a slightly distorted two-dimensional square grid (Fig. 1b). The layered structure presents a 2D (4,4) structure in which binuclear paddle-wheel unit are regarded as connected nodes and 2,6-ndc^{2-} as linkers. The 2D (4,4) network is extended into a complicated 3D framework with pillar L ligands, which employ *trans*-configuration with the Co(II)···Co(II) distance of 14.1743 Å across the L ligand, the two benzimidazole rings of a entire L ligand are parallel to each other (Fig. 1c). Topological method was used to simplify and analyze this 3D framework by TOPOS 4.0 software [23]. The Co(II) ions can be simplified as 5-connected nodes, the L ligands act as the linear linkers, the 3D framework can be represented as a binodal (4,5)-connected **xah** topology with the point symbol of $(4^2{\cdot}6^2{\cdot}8^2)(4^6{\cdot}6^4)$. In order to avoid an extremely large void space, three such identical frameworks interpenetrate each other to yield a threefold interpenetrated framework (Fig. 1d). The three-interpenetrated nets are related by a single translational vector (Class Ia) [24], with Zt = 3 and Zn = 1, where Zt represents the number of interpenetrated nets related by translation and Zn denotes the number of

Table 1 Crystallographic data and experimental details for complexes **1–2**

	1	**2**
Empirical formula	$C_{22}H_{17}CoN_2O_4$	$C_{32}H_{29}AgN_4O_4$
Formula weight	423.31	641.46
Crystal system	Triclinic	Triclinic
Space group	$P\bar{1}$	$P\bar{1}$
Unit cell dimensions		
a, Å	9.6670(3)	8.3603(7)
b, Å	9.9335(3)	9.5761(8)
c, Å	10.8896(3)	19.1928(18)
α, °	113.611(3)	95.9870(10)
β, °	101.265(3)	97.9280(10)
γ, °	97.871(2)	114.8230(10)
V, Å^3	912.36(5)	1358.6(2)
Z	2	2
ρ_{calcd} (g/cm^3)	1.574	1.568
Absorption coefficient, mm^{-1}	0.974	0.788
F(000)	444	656
Crystal size, mm	0.26 × 0.23 × 0.21	0.20 × 0.19 × 0.16
θ range, °	2.61–25.02	2.18–26.37
Index range h, k, l	−11/11, −11/11, −12/12	−10/10, −11/11, −23/23
Reflections collected	11,997	11,659
Independent reflections (R_{int})	3214 (0.0438)	5518 (0.0363)
Data/restraint/parameters	3214/0/263	5518/0/373
Goodness-of-fit on F^2	1.151	1.035
Final R_1, wR_2 ($I > 2\sigma(I)$)	0.0362, 0.0983	0.0397, 0.0764
Largest diff. peak and hole	0.573, −0.684	0.376, −0.597

Table 2 The selected bond lengths (Å) and angles (°) for complexes **1–2**

Parameter	Value	Parameter	Value
$[Co_2(2,6\text{-ndc})_2(L)]_n$ (**1**)			
Co1–O2	2.029(2)	Co1–O4	2.033(2)
Co1–O3^i	2.071(2)	Co1–N1	2.092(2)
O2–Co1–O4	161.42(17)	O2–Co1–O1^i	158.03(9)
O4–Co1–O1^i	93.04(9)	O2–Co1–O3^i	85.10(10)
O4–Co1–O3^i	158.65(9)	O1A–Co1–O3^i	86.23(9)
O2–Co1–N1	95.21(9)	O4–Co1–N1	103.01(9)
O1A–Co1–N1	105.94(9)	O3A–Co1–N1	97.68(9)
$[Ag(L)(1,4\text{–Hndc})]_n$ (**2**)			
Ag1–N3	2.194(2)	Ag1–N1	2.216(2)
Ag1–O1	2.460(2)		
N3–Ag1–N1	149.60(9)	N3–Ag1–O1	101.54(9)
N1–Ag1–O1	108.12(9)		

Symmetry code: (i) $-x$, $-y + 1$, $-z + 1$

interpenetrated nets related by crystallographic symmetry [25]. To the best of our knowledge, this is the first example of 3D cobalt(II) coordination polymer with **xah** topology [26].

3.2 Crystal Structure of $[Ag(L)(1,4\text{-Hndc})]_n$ (2)

Compound **2** crystallizes in the triclinic space group $P\bar{1}$. The asymmetric unit of compound **2** contains one Ag(I) atom, two halves of L ligand and one incompletely deprotonated 1,4-Hndc$^-$ ligand. As shown in Fig. 2a, the Ag(I) ion displays a distorted Y-shaped coordination geometry, which is occupied by two nitrogen atoms (N1, N3) from two L ligands and one oxygen atom (O1) from terminal 1,4-Hndc$^-$ ligand (Fig. 2a). Ag–O distance is 2.460(2) Å, and the Ag–N distance is Ag1–N1 = 2.216(2) Å and Ag1–N3 = 2.194(2) Å, which are all in the normal range [27, 28].

The L ligands take *trans*-conformation with $N_{donor}\cdots N\text{–}C_{sp3}\cdots C_{sp3}$ torsion angles of 180°. The N-donor ligands are μ_2-bridges coordinating to neighboring two Ag(I) centers to form a 1D "Ω"-like chain. The Ag···Ag distances across L ligands are 13.130 and 14.675 Å, respectively, and the dihedral angles between the two benzimidazole rings of the same L ligand is 0°. As shown in Fig. 2b, 1,4-Hndc$^-$ ligands show monodentate coordination mode and behave as terminal ligands connecting the "Ω"-like chain in two directions by sharing Ag(I) ions to embellish the structure of **2**. Adjacent chains are associated together through O–

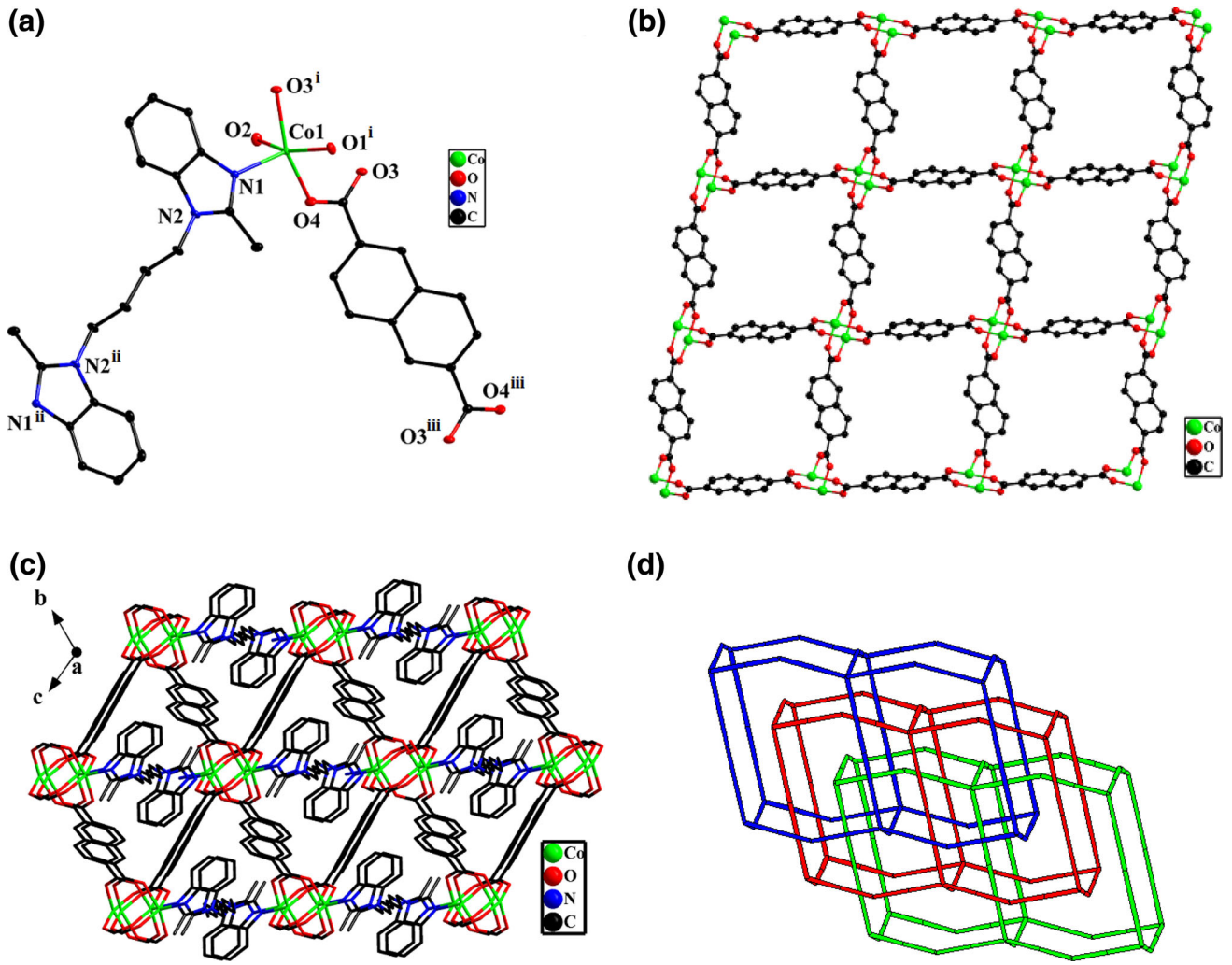

Fig. 1 The coordination environment of Co(II). Hydrogen atoms are omitted for clarity (30 % ellipsoid probability). Symmetry codes: (i) $-x, -y + 1, -z + 1$; (ii) $-x + 1, -y, -z$; (iii) $-x + 1, -y + 1, -z + 2$. **b** View of the 2D (4,4) layer connected by binuclear $[Co_2(COO)_4]$ units. **c** 3D framework of complex **1**. **d** Schematic representation of the 3D (4,5)-connected threefold interpenetrating **xah** topology for **1** (Color figure online)

H···O hydrogen bonding interactions (H3···O2^{ii} = 1.69 Å, O3–H3···O2^{ii} = 169°, symmetry code: (ii) $x, y - 1, z$) between 1,4-Hndc$^-$ ligands to generate a 2D (4,4) grid-like supramolecular network (Fig. 2c). It is worth noting that parallelogram channels are detected in the structure viewed down the a-axis with the dimension being 9.58 × 14.67 Å, which are mainly occupied by four Ag(I) ions, two L ligands and two 1,4-Hndc$^-$ anions.

3.3 IR Spectra

The IR spectra exhibit the main characteristic bands of nitrogen-containing organic ligands, and carboxylate ligands for the title complexes. The IR spectra of complexes **1** and **2** are shown in Fig. 3. There is no absorption band around 1700 cm^{-1} for **1** indicating that all carboxyl groups of the organic moieties are completely deprotonated, while the absorption band in 1690 cm^{-1} for **2** proves that 1,4-Hndc$^-$ ligand is incompletely deprotonated [27–29]. The strong peaks at 1620 and 1460 cm^{-1} for **1**, 1650 and 1420 cm^{-1} for **2**, may be attributed to the asymmetric and symmetric vibrations of carboxylate groups. The separations ($\Delta\nu[\nu_{as}(COO)–\nu_s(COO)]$) between these bands indicate the presence of bridging(160 cm^{-1} for **1**) and monodeatate (230 cm^{-1} for **2**) coordination modes of carboxyl groups. The bands in 1510 cm^{-1}(for **1**) and 1520 cm^{-1}(for **2**) are due to the $\nu_{C=N}$ absorption of the benzimidazole rings of N-containing ligands.

3.4 Thermal Properties

In order to investigate the stability of these complexes, TGA was carried out and the results are shown in Fig. 4. The TG curve of **1** exhibits two main steps of weight

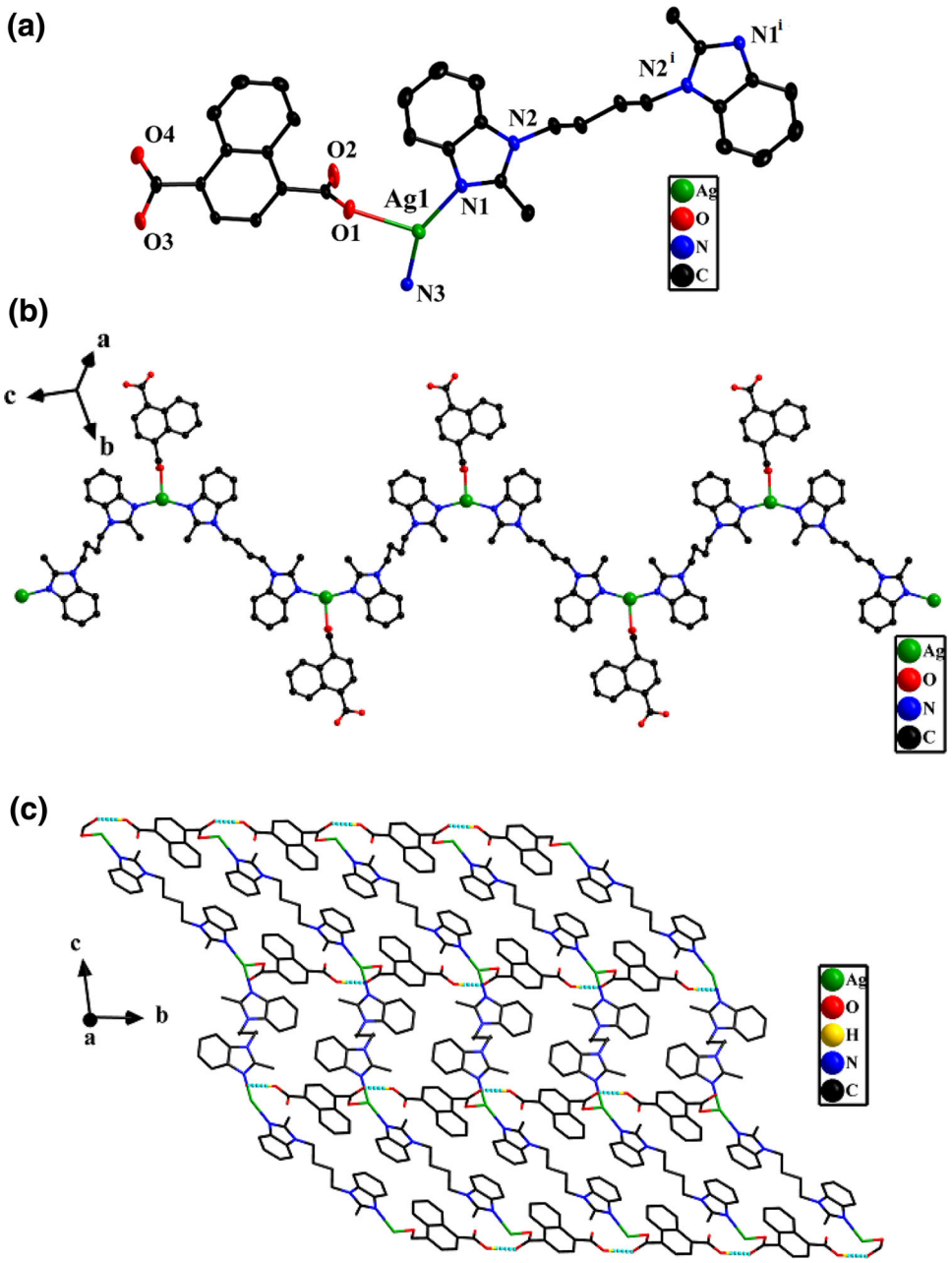

Fig. 2 **a** The coordination environment of Ag(I). Hydrogen atoms are omitted for clarity (30 % ellipsoid probability). Symmetry codes: (i) $-x, -y + 1, -z + 1$. **b** The 1D "Ω"-like chain in **2**. **c** 2D (4,4) grid-like network in complex **2**, the *blue dashed lines* represent O–H···O bonds (Color figure online)

losses. The first step started at 280 °C, which attributes to the release of L ligand. The observed weight loss of 36.6 % is close to the calculated values 36.8 %. The second step covers from 485 to 552 °C, corresponding to the release of 2,6-ndc^{2-} ligand (calcd.: 45.8 %; found: 45.9 %), the remaining weight loss of 17.5 % corresponds to CoO (calcd.: 17.4 %). However, complex **2** showed lower thermal stability. TGA indicates that chemical decomposition starts at 250 °C with the weight loss of 63.6 %, equivalent to the loss of organic ligands (calcd.: 63.8 %); the remaining weight corresponds to Ag_2O (calcd.: 36.2 %; found: 36.4 %).

3.5 Catalytic Degradation Properties

Congo red azo dye is harmful to the aquatic environment and human beings, so it is important to remove such dyes before discharging waste water. Herein, as an extension of our previous work, cobalt(II) and silver(I) complexes **1** and **2** were used as heterogeneous catalysts of the Fenton-like oxidation of congo red in the presence of hydrogen peroxide, the experiment was proceeded according to the literature [30]. As depicted in Fig. 5, when H_2O_2 alone was added into the congo red solution as the control experiment, clearly, there was no evident removal color of congo

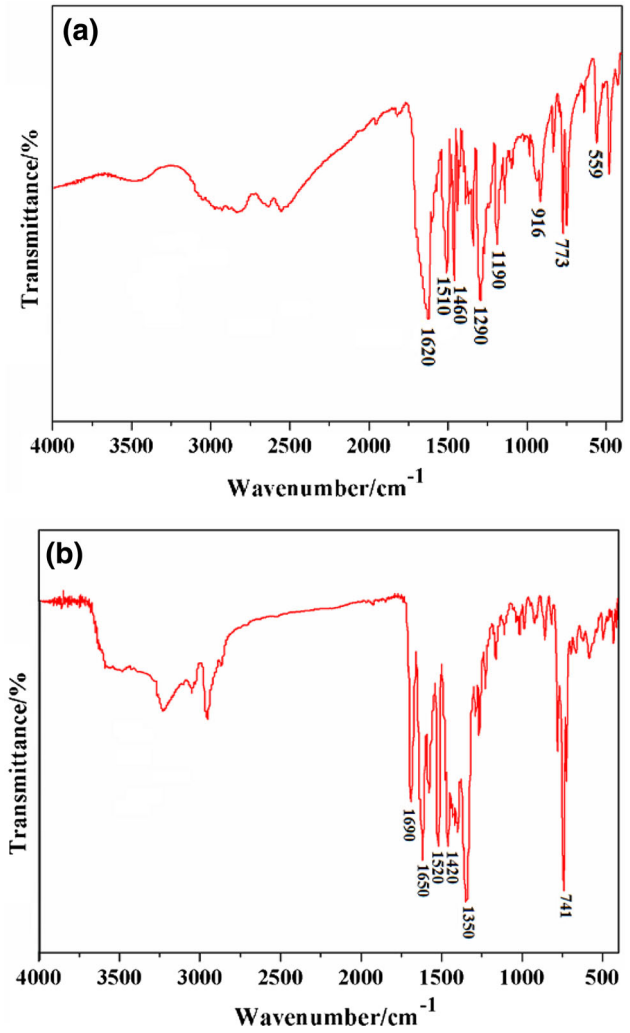

Fig. 3 **a** The IR spectrum of **1**. **b** The IR spectrum of **2**

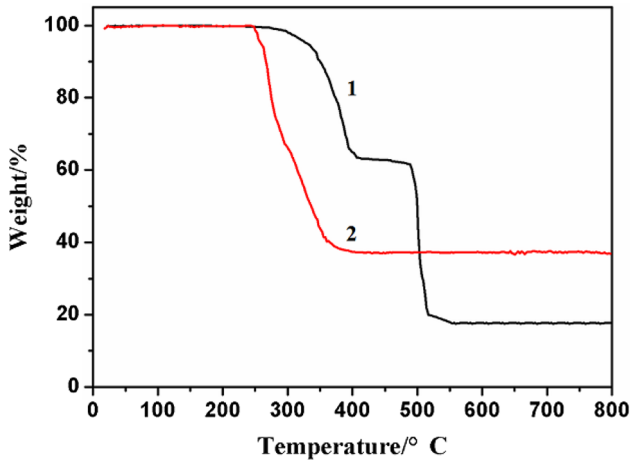

Fig. 4 TGA curves for the complexes **1** and **2**

red with the degradation efficiency of 18.6 %, indicating that congo red cannot be effectively oxidized by hydrogen peroxide. However, when adding complex **1** into the

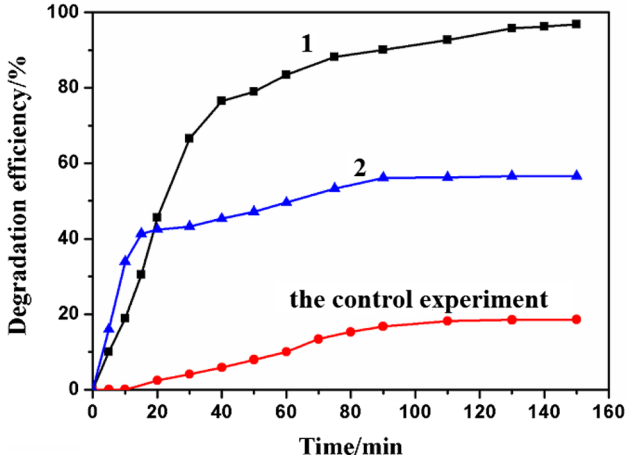

Fig. 5 Experiment results of the catalytic degradation of Congo red azo dye

system, degradation efficiency was up to 96.8 % after 150 min. However, when complex **2** was introduced into the system, only about 56.6 % of the dye was decolored. The result revealed that the complex **1** possesses a higher catalytic effect on the degradation of congo red in the Fenton-like system. The difference catalytic performances of the two complexes may be due to the distinct metal centers and the different dimensions of the coordination polymers. The complexes can catalyze hydrogen peroxide to produce ·OH radicals which are the effective and highly active oxidizing species and further increase the efficiency of the pollutant degradation significantly [31].

4 Conclusions

In summary, two new complexes based on flexible bis(benzimidazole) and aromatic dicarboxylic acids were successfully synthesized and characterized under hydrothermal conditions. The structural analysis results reveal that the coordination mode of dicarboxylic acid ligands play an important role in leading to the different topology structures of resulting coordination and supramolecular architectures. In addition, **1** shows promising catalytic activities in the decomposition of the congo red dye in a Fenton-like process.

5 Supplementary Material

CCDC 1402138 and 1407247 contain the supplementary crystallographic data for the complexes **1** and **2**. These data can be obtained free of charge via http://www.ccdc.cam.ac.uk/conts/retrieving.html, or from the Cambridge Crystallographic Data Centre, 12 Union Road, Cambridge CB2

1EZ, UK; fax: (+44) 1223-336-033; or e-mail: deposit@ccdc.cam.ac.uk.

Acknowledgments The project was supported by the National Natural Science Foundation of China (51474086), Natural Science Foundation – Steel and Iron Foundation of Hebei Province (B2015209299), the Graduate Student Innovation Fund of North China University of Science and Technology (2015S13).

References

1. T.R. Cook, Y.R. Zheng, P.J. Stang, Chem. Rev. **113**, 734 (2013)
2. J.W. Liu, L.F. Chen, H. Cui, J.Y. Zhang, L. Zhang, C.Y. Su, Chem. Soc. Rev. **43**, 6011 (2014)
3. Z.J. Lin, J. Lu, M. Hong, R. Cao, Chem. Soc. Rev. **43**, 5867 (2014)
4. G.H. Cui, C.H. He, C.H. Jiao, J.C. Geng, V.A. Blatov, Cryst. Growth Des. **14**, 4210 (2012)
5. X.L. Wang, Y. Qu, G.C. Liu, J. Luan, H. Lin, X.M. Kan, Inorg. Chim. Acta **412**, 104 (2014)
6. Z.W. Wang, M. Yu, T. Li, X.R. Meng, J. Coord. Chem. **66**, 4163 (2013)
7. C.Y. Xu, L.K. Li, Y.P. Wang, Q.Q. Guo, X.J. Wang, H.W. Hou, Y.T. Fan, Cryst. Growth Des. **11**, 4667 (2011)
8. W. Meng, Z.Q. Xu, J. Ding, D.Q. Wu, X. Han, H.W. Hou, Y.T. Fan, Cryst. Growth Des. **14**, 730 (2014)
9. Q.Q. Guo, C.Y. Xu, D.D. Zhao, Y.Y. Jia, X.J. Wang, H.W. Hou, Y.T. Fan, Z. Anorg. Allg. Chem. **638**, 868 (2012)
10. Y.Y. Liu, Y.Y. Jiang, J. Yang, Y.Y. Liu, J.F. Ma, CrystEngComm **13**, 6118 (2011)
11. J.M. Hao, H. Zhang, G.Y. Li, G.H. Cui, J. Coord. Chem. **67**, 1992 (2014)
12. E.C. Yang, Z.Y. Liu, C.H. Zhang, Y.L. Yang, X.J. Zhao, Dalton Trans. **42**, 1581 (2013)
13. H.W. Kuai, X.Y. Xu, X.C. Cheng, L.D. Feng, X.H. Zhu, J. Coord. Chem. **66**, 4304 (2013)
14. Y. Zhang, Q.F. Liu, G.E. Xing, Z.Q. Zhang, J. Mol. Struct. **1085**, 121 (2015)
15. Y. Gong, T. Wu, J. Li, J. Qin, X. Wu, R. Cao, Z. Anorg. Allg. Chem. **638**(2), 473 (2012)
16. S.S.P. Dias, V. André, J. Kłak, M.T. Duarte, A.M. Kirillov, Cryst. Growth Des. **14**, 3398 (2014)
17. X.X. Wang, Y.G. Liu, K.V. Hecke, A. Goltsev, G.H. Cui, Z. Anorg. Allg. Chem. **641**, 903 (2015)
18. J.M. Hao, B.Y. Yu, K.V. Hecke, G.H. Cui, CrystEngComm **17**, 2279 (2015)
19. R. Bronisz, Inorg. Chem. **44**(13), 4463 (2005)
20. G.M. Sheldrick, *SADABS* (University of Göttingen, Germany, 1996)
21. G.M. Sheldrick, Acta. Cryst. A. **64**, 112 (2008)
22. L. Yang, D.R. Powell, R.P. Houser, Dalton. Trans., 955 (2007)
23. V.A. Blatov, Struct. Chem. **23**(4), 955 (2012)
24. I.A. Baburin, V.A. Blatov, L. Carlucci, G. Ciani, D.M. Proserpio, J. Solid State Chem. **178**(8), 2452 (2005)
25. V.A. Blatov, L. Carlucci, G. Ciani, D.M. Proserpio, CrystEngComm **6**(65), 378 (2005)
26. X.X. Wang, Y.M. Yu, D.H. Huan, K.V. Hecke, G.H. Cui, Inorg. Chem. Commun. **61**, 24 (2015)
27. Y.Q. Yang, J. Yang, W.Q. Kan, Y. Yang, J. Guo, J.F. Ma, Eur. J. Inorg. Chem. **2013**, 280 (2013)
28. F.J. Liu, D. Sun, H.J. Hao, R.B. Huang, L.S. Zheng, J. Mol. Struct. **1014**, 70 (2012)
29. G.C. Liu, J.J. Huang, J.W. Zhang, X.L. Wang, H.Y. Lin, Transit. Met. Chem. **38**, 359 (2013)
30. H.H. Li, Y.J. Ma, Y.Q. Zhao, G.H. Cui, Transit. Met. Chem. **40**, 21 (2015)
31. M.C. Yeber, L. Díaz, J. Fernández, J. Photochem. Photobiol. A **215**, 90 (2010)